Nuclear Materials and Energy 41 (2024) 101736

Contents lists available at ScienceDirect

Nuclear Materials and Energy

journal homepage: www.elsevier.com/locate/nme

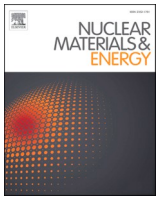

SOLPS-ITER modeling of divertor detachment in MAST-U's super-X double null configuration and comparison to experiment

R. Maurizio [a,*], A.W. Leonard [a], J.H. Yu [a], J. Harrison [b], K. Verhaegh [b], N. Lonigro [b,c], A.G. McLean [d]

[a] General Atomics, San Diego, CA 92186, USA
[b] UKAEA, Culham Science Campus, Abingdon, Oxfordshire OX14 3DB, United Kingdom
[c] York Plasma Institute, University of York, United Kingdom
[d] Lawrence Livermore National Laboratory, Livermore, CA 94550, USA

A B S T R A C T

The MAST-U tokamak has recently undergone upgrades to investigate any detachment advantages of the "Super-X Double-Null" magnetic configuration, a concept featuring up-down symmetry with two magnetic nulls and elongated divertor legs with strong wall baffling. This study presents SOLPS-ITER simulations of MAST-U Super-X Double Null discharges, in H-mode conditions, compared to initial 2D imaging measurements of divertor detachment characteristics. In the simulations, the Super-X divertor targets achieve detachment at a substantially lower upstream separatrix density compared to a shorter leg, conventional configuration (CD). As the density increases further in the Super-X configuration, the cold detached front moves upstream towards the X-point. Its speed in the poloidal plane, calculated as the change in front location divided by the corresponding increase in upstream plasma density, decreases by a factor of ~ 3–4 as the front transitions from the baffled divertor chamber to the main plasma chamber, reaching a speed comparable to that observed in the CD configuration. In a chosen experimental Super-X density ramp discharge, the ionization front, identified using D_2 Fulcher emission as a proxy, is already displaced from the target at the start of the divertor fueling ramp, whereas modeling of the same initial phase shows the ionization front still close to the target. As divertor fueling increases, both experiment and modeling show the ionization front moving further upstream towards the divertor throat. However, the associated variation in upstream density is ~ 2 times larger in the modeling compared to the experiment, resulting in a broader detachment window. Comprehensive modeling efforts are underway to address these discrepancies, with several inaccurate modeling assumptions identified as potential causes of the deviation.

1. Introduction

The safe steady-state operation of a nuclear fusion tokamak power plant will require operation of the divertors in the so-called "detached" regime, characterised by substantial radiative losses within the divertor volume, which effectively reduce the plasma temperature in the divertor, lowering the plasma power and particle fluxes to levels acceptable for divertor plate integrity. Accessing this regime involves increasing either the plasma density or introducing low-Z impurities, as both mechanisms enhance volumetric radiation and lower the plasma temperature in the edge. Detachment onset is often defined as when the target electron temperature falls below approximately 5 eV, or when the ion flux to the target rolls-over [1]. Continuing to increase the density results in the cold plasma front, referred to in this study as the "detachment front", moving away from the divertor plate towards the magnetic X-point. This movement is associated with a further beneficial decrease in energy and particle fluxes directed to the divertor plates. However, once the cold plasma front reaches the X-point, it frequently leads to undesired core performance degradation and, in extreme cases, a radiative collapse of the plasma. Therefore, maintaining the detachment front at an intermediate position between the divertor plate and the X-point is a potential strategy to optimize both divertor conditions and core performance simultaneously.

Experiments conducted using the conventional short-legged "Single Null" magnetic configuration in multiple tokamak devices have revealed the considerable challenge of maintaining the detachment front between the target and the X-point [2 3 4]. This difficulty arises from the narrow range in plasma density or impurity fraction required to shift the detachment front from the target to the X-point, known as the "detachment window". A narrow detachment window indicates the high sensitivity of the detachment front to changes in plasma density or impurity fraction, making it prone to swift movements from the divertor plate to the X-point due to minor perturbations in density or impurity fraction. This presents a significant challenge for control algorithm development and underscores the need to explore alternative approaches for expanding the detachment window.

* Corresponding author.
E-mail address: maurizior@fusion.gat.com (R. Maurizio).

https://doi.org/10.1016/j.nme.2024.101736
Received 17 May 2024; Received in revised form 6 August 2024; Accepted 10 September 2024
Available online 13 September 2024

Advanced magnetic configurations with elongated divertor legs are anticipated to offer a broader detachment window compared to conventional magnetic configurations, leading to enhanced controllability [5 6 7]. Several experimental facilities have either implemented or are in the process of upgrading their hardware to investigate this potential. In the United States, the DIII-D tokamak has launched a multi-stage divertor program aimed at advancing research on core–edge integration to qualify scenarios for a fusion pilot plant. The current (first) phase involves a relatively shallow divertor to maximize plasma volume for advanced tokamak scenarios. The subsequent (second) phase will introduce a deeper divertor structure to operate "unconventional" Single-Null plasmas with elongated divertor legs, aiming to stabilize the detachment front between the divertor plate and the X-point. In the United Kingdom, the MAST-U tokamak has recently undergone upgrades to comprehensively investigate the potential detachment advantages of the Super-X Double-Null magnetic configuration [8 9 10]. The Double-Null (DN) feature entails up-down symmetry in the magnetic configuration, with two magnetic nulls, aiming to evenly distribute exhaust heat and particles between upper and lower divertor structures. The "Super-X" (SX) feature involves placing the divertor plate at a notably larger major radius than the conventional configuration, elongating the divertor leg [11]. Additionally, the majority of the leg is surrounded by strong wall baffling to enhance neutral trapping, effectively forming an upper and a lower "divertor chamber," as later illustrated in Fig. 1.

This paper contributes to the ongoing international research on elongated divertor legs by conducting a series of numerical simulations of MAST-U Super-X Double Null plasmas, analyzing experimental measurements, and comparing them to boundary modeling. These plasmas operate in the high-confinement mode (H-mode) and detachment is achieved by gradually increasing the plasma density and divertor neutral pressure without extrinsic impurities. The paper is structured as follows: Section 2 presents SOLPS-ITER modeling of a plasma density ramp, utilizing actual MAST-U equilibria from both a Super-X and Conventional DN discharge. Then, Section 3 details the modeling of a particular Super-X density ramp discharge, comparing simulation outcomes to experimental measurements of the detachment front location. Each section includes discussions of the results and outlook, with a summary provided in Section 4.

2. Detachment in super-X vs conventional configuration: Modeling

Initial modeling compares the MAST-U Super-X DN configuration (SXD) to a more conventional short-leg DN configuration, referred to as "Conventional Divertor" (CD). Simulations are run using the SOLPS-ITER 3.0.8 code package [12], which couples the 2D multi-fluid plasma transport code B2.5 and the 3D kinetic neutral transport code EIRENE. Particle drift effects are not included. The SOLPS-ITER computational meshes are built using MAST-U plasma discharges, shot 47,608 at 0.53 s (CD) and shot 47,577 at 0.53 s (SXD), see Fig. 1a-b. The plasma grid extends to R-R_{sep} ~ 40 mm in the Scrape-Off Layer, which corresponds to approximately 13 times the heat flux width based on the ITPA H-mode scaling [13]. This large width is chosen to ensure that the grid can contain the entire exhausted power and that the plasma solution remains largely unaffected by the boundary conditions set at the far-SOL side. The modelled plasma comprises all charged states of deuterium and carbon, with the walls and targets made of carbon. The plasma current is 0.8 MA and the power injected at the grid pedestal boundary is 3 MW (maximum available heating power), equally split between electrons and ions. The recycling coefficient is set to 100 % on all wall elements, with standard pre-sheath boundary conditions. One pumping surface is placed in each divertor chamber, see Fig. 1a, with a recycling coefficient of 98.955 %, as used in previous MAST-U SOLPS-ITER simulations [14]. The anomalous transport coefficients in both the CD and SXD simulations, shown in Fig. 1e, are estimated by matching plasma radial profiles of electron density and temperature measured by MAST-U Thomson scattering system for a similar but better diagnosed Super-X plasma (shot 48133), see Fig. 1c-d, as explained in [15]. Some radial adjustment of the profiles is typically necessary due to significant

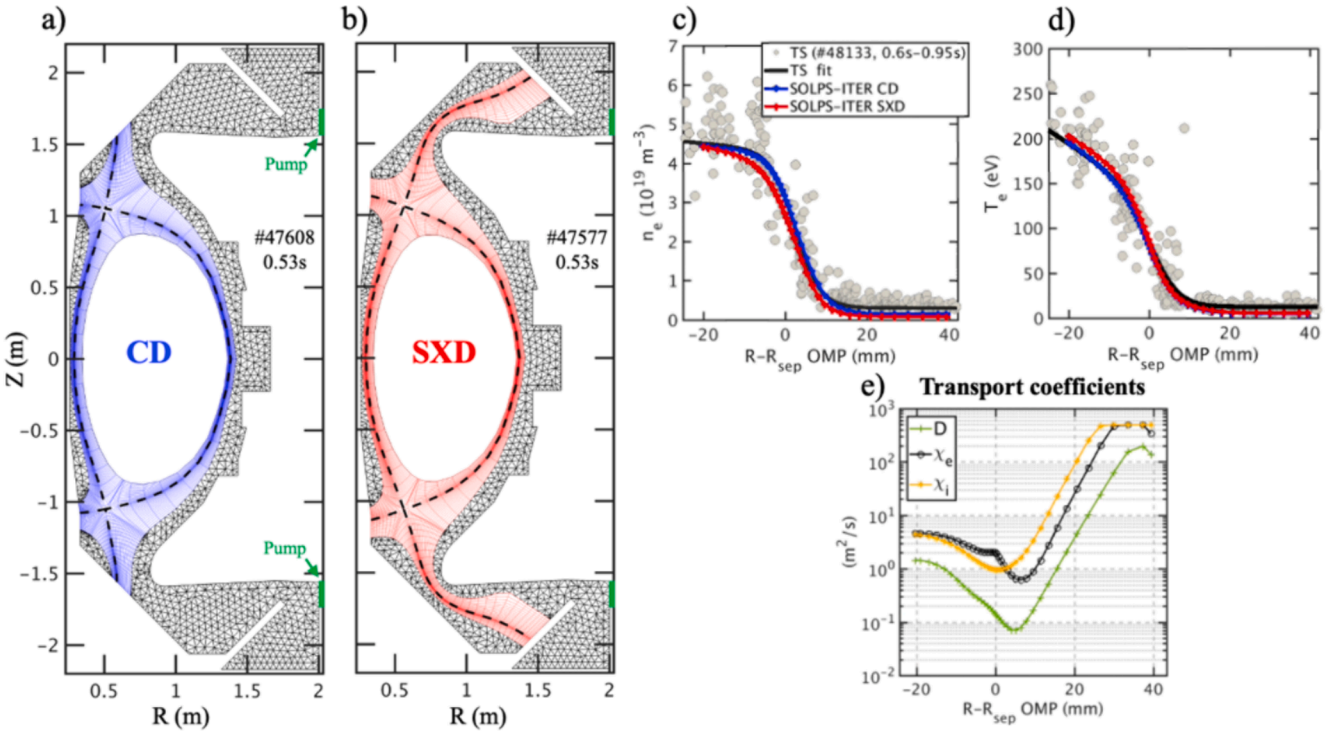

Fig. 1. SOLPS-ITER mesh of a MAST-U Conventional DN (a) and Super-X DN (b) configuration. (c-d) MAST-U outboard mid-plane electron density and temperature profiles, measured by a Thomson Scattering system, fitted with a modified hyperbolic tangent function and compared to SOLPS-ITER simulations. (e) Anomalous transport coefficients adopted in both the CD and SXD simulations, estimated by matching the plasma profiles shown in (c-d).

uncertainties affecting the magnetic reconstruction of the separatrix position. In this study, the plasma profiles are shifted by 8.3 mm to achieve a value of approximately 85 eV at the separatrix, estimated through power balance considerations [16]. This constraint on the model results in a Scrape-Off Layer (SOL) heat flux width of approximately 3.2 mm, fitted at the outboard mid-plane, in good agreement with the ITPA H-mode scaling (~3.4 mm [13]), but falls below predictions from a MAST-specific H-mode scaling (~6 mm [17]) as well as recent MAST-U measurements in the CD configuration [18]. Note that these transport coefficients lead to relatively small power fluxes reaching the first wall (4 % to 10 % of the power crossing the magnetic separatrix). To facilitate numerical convergence, density is controlled by prescribing a value for the ion density at the grid pedestal boundary, which the code achieves by regulating the amount of injected ion flux at that boundary. A more detailed description of all the adopted SOLPS-ITER boundary conditions can be found in [19 20]. For the presented set of simulations, the injected particle source is typically in the range of 10^{20} to 10^{22} D^+/s. Results are exclusively presented for the lower divertors, as the upper divertors behave in a similar way due to the magnetically up-down symmetric nature of these Double-Null configurations and the absence of particle drift effects in these simulations.

In the simulated density scan, the Super-X divertor targets achieve detachment at a substantially lower upstream separatrix density compared to the shorter leg, conventional configuration, specifically at 1.4 10^{19} m^{-3} vs 7 10^{19} m^{-3} for the outer targets (around 80 % reduction), and at 3.5 10^{19} m^{-3} vs 5 10^{19} m^{-3} for the inner targets (around 30 % reduction), see Fig. 2a-c. The density at which the detachment front (defined in this work as the $T_e = 10$ eV front) reaches the X-point is the same for Super-X and Conventional configuration, around 3 10^{20} m^{-3}, see Fig. 2b-d. Consequently, SOLPS-ITER shows that the detachment window, defined as the range in plasma density required to shift the detachment front from the target to the X-point, is approximately 25 % broader in the Super-X compared to the Conventional configuration. In the Super-X configuration, the sensitivity of the detachment front position to upstream density variation changes significantly between the divertor chamber and the main chamber, see Fig. 2d. The detachment front moves at an approximate poloidal speed of 12 cm for each 10^{19} m^{-3} variation in upstream separatrix electron density. This speed sharply decreases to approximately 3 cm/10^{19} m^{-3} in the main chamber. A similar trend is observed for the speed parallel to the SOL magnetic field lines, which decreases from approximately 0.6 m/10^{19} m^{-3} in the divertor chamber to around 0.1 m/10^{19} m^{-3} in the main chamber. Interestingly, the front speed in the main chamber closely resembles that observed for the CD configuration, shown in Fig. 2b. In the CD configuration, the detachment front moves at a poloidal speed of around 2 cm/10^{19} m^{-3}, corresponding to approximately 0.2 m/10^{19} m^{-3} in the parallel direction.

The observed slow-down of the detachment front when approaching the divertor throat agrees with previous SOLPS-ITER modeling of MAST-U Super-X discharges [21], and it can be interpreted as the effect of changes in the magnetic field line geometry. The divertor throat corresponds to a zone of elevated parallel gradient in the total magnetic field, where the magnetic field intensity rapidly increases as the detachment front moves up the flux tube, resulting in a reduction of the flux tube cross-sectional area. Consequently, a greater parallel heat flux density must be dissipated as the detachment front progresses upstream, necessitating a larger variation in upstream density to move the front further up the flux tube.

However, the sharp change in speed as the front crosses the narrow divertor chamber throat indicates an additional effect associated to the substantial difference in wall baffling between the divertor chamber and the main plasma chamber. When the detachment front is inside the

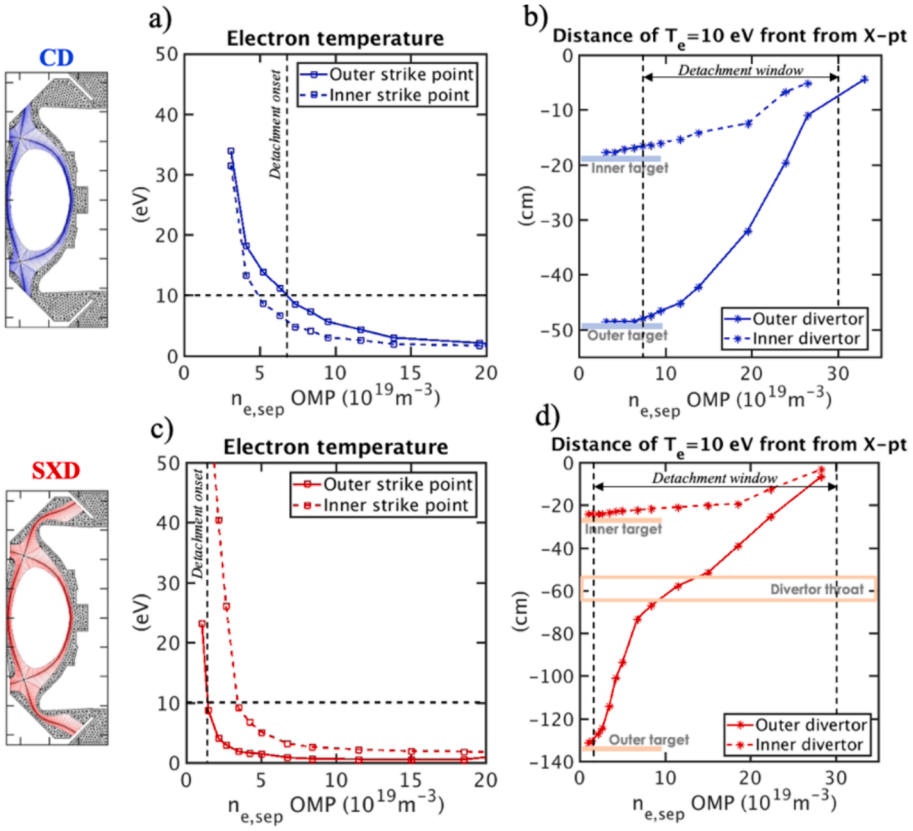

Fig. 2. (a-c) For the lower divertors, simulated electron temperature at the outer strike point (solid line) and inner strike point (dashed line) as a function of outer mid-plane separatrix electron density. (b-d) Poloidal distance of the simulated $T_e = 10$ eV front from the X-point, measured along the mesh first flux tube in the SOL, in the outer (solid line) and inner (dashed line) lower divertor.

divertor chamber, the significant neutral trapping implies that a minor variation in upstream density is sufficient to move the front up the flux tube. Conversely, when the front is in the main chamber, the weaker neutral trapping implies that a larger variation in upstream density is needed to achieve the same advancement of the front up the flux tube.

3. Detachment in super-X configuration: Comparison of modeling to experiment

Subsequent modeling focuses on the MAST-U Super-X H-mode discharge 49323 (and diagnostic repeat discharge 49324), where plasma density and divertor neutral pressure are gradually raised using valves in the two divertor chambers. This new Super-X configuration differs from that presented in the previous section. Specifically, the plasma is more elongated, with X-points closer to the floor and ceiling, resulting in a shortening of the outer divertor legs by around 7 cm in the poloidal plane. Also, the flux surfaces at the outer targets exhibit a significantly larger incidence angle and lower flux expansion. The power injected at the grid pedestal boundary is also lower, reduced to 2 MW from 3 MW, as determined through measurements of Ohmic power, Neutral Beam Injection power, and core radiation from bolometry obtained from an equivalent plasma shot (49320). Consequently, a new computational mesh is constructed using the equilibrium reconstruction of shot 49323 at 0.7 s, shown in Fig. 3a. New anomalous transport coefficients are calculated using Thomson Scattering measurements of pedestal electron density and temperature profiles from the start of the density ramp (t = 0.47 s-0.53 s), see Fig. 3b-c-d. These profiles have been radially adjusted to achieve ~ 85 eV at the separatrix, as discussed earlier. Like the previous case, these calculations yield a SOL heat flux width of 3.2 mm at the plasma outboard mid-plane, aligning again with the ITPA H-mode scaling prediction of approximately 3.6 mm but falling below the MAST-specific scaling prediction, and recent MAST-U measurements, of approximately 6 mm.

In the simulated density scan, the Super-X divertor targets achieve detachment at density values comparable to those observed in the previously presented 3 MW Super-X case (1.3 10^{19} m^{-3} for the outer targets and 4.5 10^{19} m^{-3} for the inner targets), see Fig. 4a. At higher plasma densities, the detachment front moves at a poloidal speed of approximately 14 cm/10^{19} m^{-3} in the divertor chamber and 4 cm/10^{19} m^{-3} in the main chamber, mirroring the behaviour of the Super-X configuration described in the previous section, see Fig. 5b. In the direction parallel to the SOL magnetic field line, the front moves at approximately 0.6 m/10^{19} m^{-3} in the divertor chamber and 0.2 m/10^{19} m^{-3} in the main chamber.

A preliminary comparison of modeling to experiments is presented here. In the experiment, the detachment front is tracked by observing the D_2 Fulcher band emission (595–605 nm), which serves as a proxy for the divertor ionization source. These measurements are obtained using a Multi-Wavelength Imaging system (MWI) [22 9]. At the beginning of the experimental density ramp (t ~ 0.5 s), the ionization front (bright D_2 Fulcher emission) appears already displaced from the target (Fig. 5a), indicating detachment of the divertor target. However, modeling of the same initial phase of the discharge (t = 0.47 s-0.53 s) shows the ionization front and D_2-associated Fulcher emission still located close to the target (Fig. 5d-5 g). With an increase in divertor fueling, the experimentally measured ionization front moves further upstream towards the divertor throat (Fig. 5b-c), signalling progression to a deeper detached state, and eventually exits the field of view of the MWI system. A similar progression is observed in the simulations (Fig. 5d-5f and 5g-5i), but the associated variation in upstream separatrix density is much larger than observed in the experiment. Specifically, the movement of the detachment front from the middle to the throat of the divertor chamber requires just a ~ 60 % increase in separatrix density in the experiment (compare Fig. 5a-5c), whereas it necessitates a ~ 120 % increase in separatrix density in the simulations (compare Fig. 5e-5f). Note that the increase in separatrix density in the experiment has large uncertainty due to significant scatter in the Thomson data.

Comprehensive modeling efforts are currently underway to address the discrepancy in detachment density and detachment window between experiment and simulations. Several possibly inaccurate assumptions in the simulation have been identified as potential causes of the deviation. A primary improvement is expected by reducing the power injected at the grid pedestal boundary from 2 MW to approximately 1.25 MW, a value observed in similar H-mode discharges.

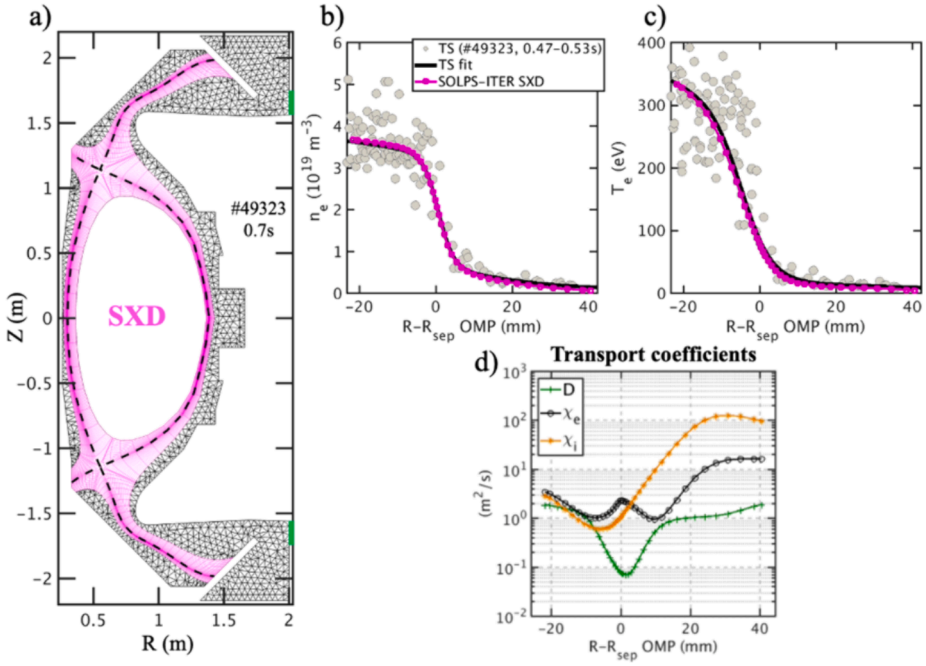

Fig. 3. (a) SOLPS-ITER mesh of a Super-X DN configuration. (b-c) MAST-U outboard mid-plane electron density and temperature profiles, measured by a Thomson Scattering system, fitted with a modified hyperbolic tangent function and compared to SOLPS-ITER simulations. (d) Anomalous transport coefficients adopted in the simulations, estimated by matching the plasma profiles shown in (b-c).

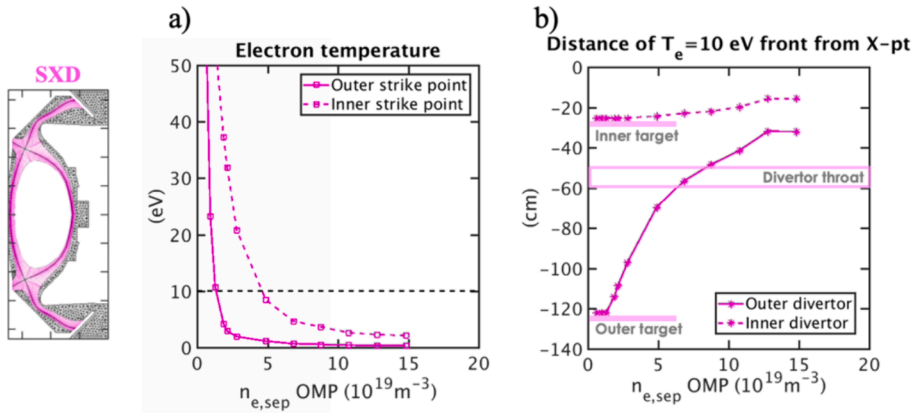

Fig. 4. (a) For the lower divertor, electron temperature at the outer strike point (solid line) and inner strike point (dashed line) as a function of outer mid-plane separatrix electron density. (b) Poloidal distance of the $T_e = 10$ eV front from the X-point, measured along the mesh first flux tube in the SOL, in the outer (solid line) and inner (dashed line) lower divertor.

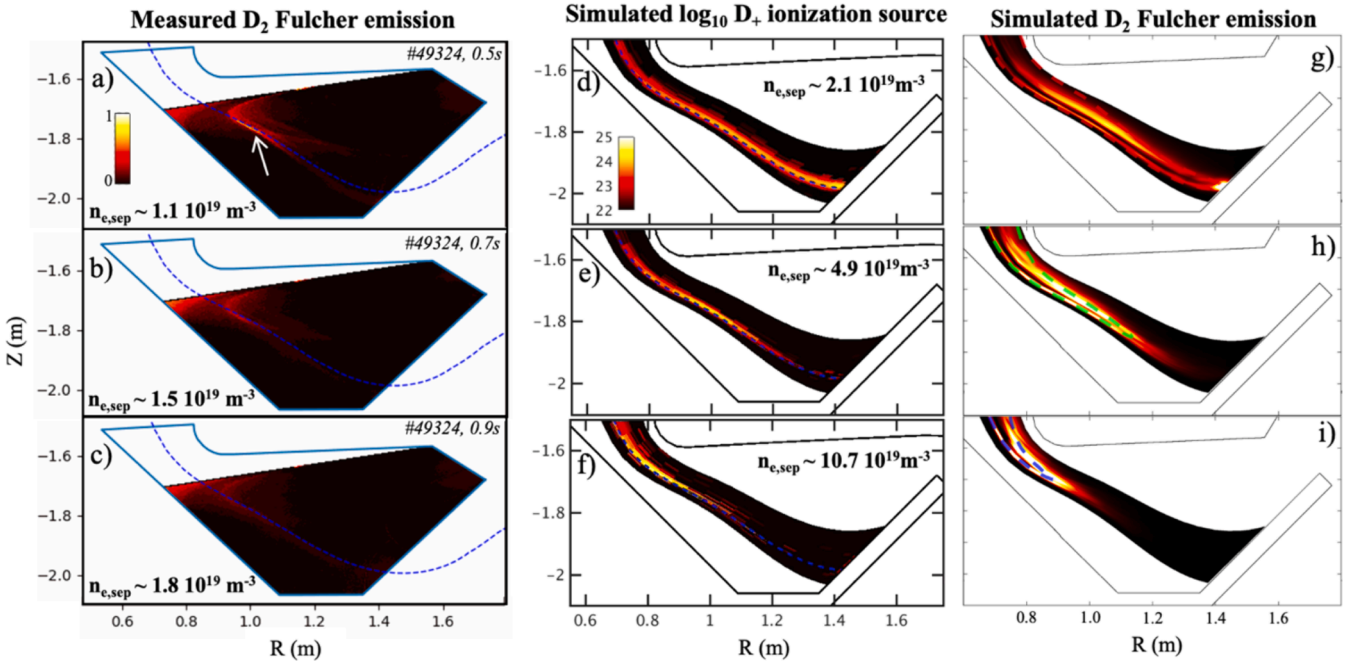

Fig. 5. (a-c) Normalized D_2 Fulcher emission as measured by MAST-U's MWI system at different times during a plasma density ramp. SOLPS-ITER simulation of deuterium ionization source (d-f) and normalized D_2 Fulcher emission (g-i) for progressively increasing value of plasma density. The magnetic separatrix is shown as a dashed blue line. In (g-i), dashed lines indicate the 4 eV contour. (For interpretation of the references to colour in this figure legend, the reader is referred to the web version of this article.)

Consequently, the assumed temperature at the separatrix will be adjusted from 85 eV to approximately 50 eV [18]. Secondary improvements are expected by implementing a more precise fueling scheme in the simulations, incorporating constant fueling from the High Field Side (HFS) wall along with a ramped fueling from inside both divertor chambers. Furthermore, including the effect of particle drifts, typically minor at these low powers, may lead to further refinements.

4. Summary and conclusions

This paper presents SOLPS-ITER simulations of MAST-U Super-X (SXD) and Conventional (CD) Double Null discharges in H-mode conditions, along with a preliminary comparison to 2D divertor imaging measurements. The simulations show that SXD outer targets detach at a much lower upstream separatrix density than CD. As the detachment front moves upstream towards the X-point, its speed in the poloidal plane (change in front location divided by corresponding increase in upstream plasma density) decreases by a factor of 3–4 when transitioning from the baffled divertor chamber to the main plasma chamber. This sharp slowdown is attributed to changes in magnetic field line geometry (parallel gradient of the magnetic field) and significant differences in wall baffling between the divertor and the main plasma chamber. The comparison of SXD modeling to experimental data shows mixed agreement, with the model overestimating the density required for detachment onset and the upstream density variation needed to move the detachment front to the X-point. Potentially inaccurate assumptions in the simulation, such as excessive power injected at the grid pedestal boundary and an inaccurate fueling scheme, have been identified, and further modeling efforts are underway.

Disclaimer

This report was prepared as an account of work sponsored by an agency of the United States Government. Neither the United States

Government nor any agency thereof, nor any of their employees, makes any warranty, express or implied, or assumes any legal liability or responsibility for the accuracy, completeness, or usefulness of any information, apparatus, product, or process disclosed, or represents that its use would not infringe privately owned rights. Reference herein to any specific commercial product, process, or service by trade name, trademark, manufacturer, or otherwise does not necessarily constitute or imply its endorsement, recommendation, or favoring by the United States Government or any agency thereof. The views and opinions of authors expressed herein do not necessarily state or reflect those of the United States Government or any agency thereof.

CRediT authorship contribution statement

R. Maurizio: Writing – original draft, Software, Methodology, Formal analysis, Conceptualization. **A.W. Leonard:** Supervision, Project administration, Funding acquisition, Conceptualization. **J.H. Yu:** . **J. Harrison:** Resources, Project administration. **K. Verhaegh:** Resources, Investigation. **N. Lonigro:** Resources. **A.G. McLean:** Supervision.

Declaration of competing interest

The authors declare that they have no known competing financial interests or personal relationships that could have appeared to influence the work reported in this paper.

Data availability

Data will be made available on request.

Acknowledgements

This material is based upon work supported by the U.S. Department of Energy, Office of Science, Office of Fusion Energy Sciences, under Award(s) DE-SC0018991.

References

[1] A. Loarte, Nucl. Fusion. 38 (1998) 331.
[2] T. Ravensbergen, Nat. Commun. 12 (2021) 1105.
[3] D. Eldon, Nucl. Mater. Energy. 27 (2021) 100963.
[4] M. Bernert, Nucl. Fusion. 61 (2021) 024001.
[5] G. Fishpool, J. Nucl. Mater. 438 (2013) S356–S359.
[6] M. Wigram, Nucl. Fusion. (2019) 59.
[7] M. Umansky, Nucl. Fusion. (2020) 60.
[8] K. Verhaegh, Nucl. Fusion. 63 (2023) 016014.
[9] T.A. Wijkamp, Nucl. Fusion. 63 (2023) 056003.
[10] E. Havlickova, Plasma Phys. Control. Fusion. 57 (2015) 115001.
[11] P.M. Valanju, Phys. Plasmas 16 (2009) 056110.
[12] X. Bonnin, Plasma and Fusion Research, 2016, 11.
[13] T. Eich, Nucl. Fusion. 53 (2013) 093031.
[14] A. Fil, Nucl. Fusion. 62 (2022) 096026.
[15] J.M. Canik, J. Nucl. Mater. 435 (2011) S409–S412.
[16] P.C. Stangeby, Nucl. Fusion. 55 (2015) 093014.
[17] A.J. Thornton, Nucl. Fusion. 56 (2014) 055008.
[18] J. Harrison, Plasma Phys. Controlled Fusion. Accepted, 2024.
[19] R. Maurizio, Nucl. Fusion. (2021) 61.
[20] R. Maurizio, Nucl. Mater. Energy. 34 (2023) 101356.
[21] O. Myatra, Nucl. Fusion. 63 (2023) 096018.
[22] X. Feng, Rev. Sci. Instrum. 92 (2021) 063510.